Korean J. Chem. Eng., 35(1), 272-282 (2018)
DOI: 10.1007/s11814-017-0270-3

pISSN: 0256-1115
eISSN: 1975-7220

Improvement of capacitive deionization performance via using a Tiron-grafted TiO_2 nanoparticle layer on porous carbon electrode

Byeong Ho Min, Jae-Hwan Choi, and Kyeong Youl Jung†

Department of Chemical Engineering, Kongju National University,
1223-24 Cheonan-daero, Seobuk-gu, Cheonan, Chungnam 31080, Korea
(*Received 7 August 2017 • accepted 25 September 2017*)

Abstract−A novel ion-selective inorganic-carbon composited electrode was designed to improve the performance of a capacitive deionization (CDI) process. Disodium 4,5-dihydroxy-1,3-benzenedisulfonate (Tiron) was grafted on the surface of titania nanoparticles, and a thin titania layer with a thickness of 10-12 μm was formed on porous activated-carbon (AC) electrode and used as the negative electrode in a CDI full cell. The resulting Tiron-grafted titania nanoparticles showed an excellent ion-exchange capacity (1.51 meq/g). As a result, the Tiron-titania/AC composited electrode was found to have improved desalination properties in terms of specific adsorption capacity, specific adsorption rate and current efficiency compared with the pristine CDI electrode. Improved desalination performance was attributed to a reduction in co-ion expulsion effect by ion-exchangeable functional groups in Tiron-grafted titania. In addition, the improved desalination performance through the introduction of a porous layer of Tiron-grafted titania was similar to that of the conventional membrane capacitive deionization (MCDI) using an ion-exchange membrane. From the results obtained, it has been experimentally proven that the use of Tiron-grafted TiO_2/AC composite as the negative electrode in the CDI process is a simple and effective way to achieve high desalination performance.

Keywords: Capacitive Deionization, Tiron, TiO_2, Ion Selectivity, Porous Carbon

INTRODUCTION

Capacitive deionization (CDI) technique has gained great attention as a potential process for the desalination of sea or brackish water and the removal of ionic contaminants in water [1-5]. Compared with the conventional desalination processes, including reverse osmosis, electrodialysis and evaporation, the CDI technique is energy-efficient and environmentally-friendly because it can be operated at a low electrical potential, requires no chemicals and produces no by-products [1,3,6]. Basically, CDI is operated on the same principle as the electric double-layer capacitor (EDLC) [7]. That is, it involves the adsorption of charged ions on the surface or in the pores of electrode materials when the external voltage is applied, and the ions are desorbed reversibly when the voltage is removed or reverse. The difference between EDLC and CDI is whether the electrolyte flow exists or not. In EDLC, there is no electrolyte flow [8]. On the contrary, the electrolyte solution (brine) in CDI flows through the channel between two electrodes [9].

The performance of CDI is strongly affected by the characteristics of electrode materials [10-12]. To achieve large salt adsorption, the electrode materials should have large surface area, proper pore structure, good electrical conductivity and suitable surface characteristics for the adsorption of charged ions [13,14]. Given this, carbon-based porous materials including activated carbon (AC) [15-18], carbon aerogel [19-21], carbon nanotube [22-24] and graphene [25-28] have been investigated as the electrode of CDI. The salt-removal performance of CDI also strongly depends on the adsorption-desorption property in the electrical double layer (EDL) even if the same carbon materials are used. In the CDI structure, the adsorption of ions occurs in the EDL formed near the carbon surface. When the electric potential is applied, counter-ions are absorbed on the electrode surface, whereas co-ions are expelled out [29-31]. This co-ion expulsion is the main reason for lowering the desalination efficiency of CDI. Thus, many efforts have been dedicated to overcome this drawback of the conventional CDI.

There are three approaches to solving the weaknesses of CDI. The first is to use free-standing ionic exchange membranes in front of the electrodes, which is called membrane-capacitive deionization (MCDI) [32-34]. The ion-exchange membrane can move counter-ions to the electrodes more effectively. As a result, the expulsion effect of co-ions can be reduced, resulting in substantial improvement in the salt removal efficiency as well as the charge efficiency. The use of free-standing ion-exchange membranes, however, increases the bulk resistivity of the whole unit due to the weak contact between the electrodes and the membranes. The second approach is to directly modify the surface of carbon with ion-selective functional groups such as charged sulfonic or amine groups [35-41]. Then, the functional groups act positively to increase the specific ionic sorption capacity because they can reduce the co-ions expulsion and increase the wettability or hydrophilicity of the electrode surface. The third approach is to form a polymer film having the ion-exchange ability on the electrode [42-47]. The ion-exchange polymer film can successfully do the same role as

†To whom correspondence should be addressed.
E-mail: kyjung@kongju.ac.kr

the ion-exchange membrane in MCDI. In addition, the good contact characteristics between the polymer film and the electrode are helpful for achieving lower contact resistance compared with the MCDI using the free-standing ion-exchange membranes. In terms of the ion selectivity or the ion transportation, the ion-exchange polymer film should have the functional groups as much as possible. The concentration of hydrophilic functional groups on the polymer, however, is limited because the ion-exchange polymer can be soluble in water or swelled largely so that a uniform film is hard to be formed. Thus, the design of new ion-exchange film with a porous structure having high ion-exchange ability is a challenging work for the development of high-performance CDI.

In this work, an inorganic porous film consisting of nanoparticles having an ion selective functional group was introduced on the activated carbon (AC) electrode in order to improve the CDI performance. Disodium 4,5-dihydroxy-1,3-benzenedisulfonate (Tiron) was grafted to the surface of titania nanoparticles. A porous and ion-exchangeable titania film was formed by a screen printing technique on the activated carbon (AC) layer of the negative electrode. Then, the sulfonic groups of Tiron made it possible to give the function of cation exchange to the titania porous film. Unlike the ion exchange polymer membrane, the inorganic membrane has hydrophilic and ion-exchangeable functional groups and does not cause a problem of being dissolved in water. To our best knowledge, there has been no attempt to improve CDI performance using ion selective inorganic films. To experimentally prove the possibility of Tiron-grafted titania layer as a ion-exchangeable film, the deionization performance of the carbon electrode having the Tiron-grafted TiO_2 layer was compared with the conventional CDI and MCDI cells. Finally, we found that the introduction of the Tiron-grafted TiO_2 layer enhances the desalination performance when compared with the conventional CDI structure.

EXPERIMENTAL

1. Materials

Titania nanopowder (primary particle size <25 nm) and disodium 4,5-dihydroxy-1,3-benzenedisulfonate (Tiron) were purchased from Aldrich and used without further purification. Activated carbon powder (CEP-21K) was supplied by Power Carbon Technology Co., Korea, and used as the electrode materials. Graphite sheets of 250 μm in thickness were supplied by Dongbang Carbon Co., Korea, and used as the current collector. PVdF (Polyvinylidene fluoride, Aldrich) and DMAc (N,N-Dimethylacetamide, Aldrich) were used as the binder and the solvent for the preparation of carbon paste, respectively. Commercial ion-exchange membranes (Neosepta AMX and CMX) were purchased from Astom Co., Japan. Nylon net with 100 μm in thickness was used as a spacer inserting between two electrodes in CDI or MCDI cells.

2. Synthesis and Characterization of Tiron-grafted TiO_2 Nanoparticles

2-1. Synthesis

Tiron has two sulfonic acid groups (-SO_3Na) and hydroxyl groups (-OH) per molecule. Catecholic derivatives are known to easily form a stable Ti-catecholic salt chelate complex at room temperature. So, Tiron is a proper reagent for the sulfonation of titania surface. The chemisorption of Tiron on the surface of TiO_2 nanoparticles was carried out by the following procedure. First, HCl aqueous solution of pH=2.0 was prepared by adding HCl into purified water. Next, TiO_2 particles (5 g) were dispersed into the HCl aqueous solution of 200 mL, and 2.5 g of Tiron was dissolved in the HCl aqueous solution of 300 mL. These two solutions were mixed well by using a magnetic stirrer for 30 min at room temperature. Thereafter, the Tiron-grafted TiO_2 powders were withdrawn by a filtration process and washed several times until the washed solution reached neutral pH. Finally, the withdrawn Tiron-grafted TiO_2 powders were dried in a convection oven at 40 °C for 24 h.

2-2. Characterization

The surface functional groups grafted on the titania surface were monitored by FT-IR and TGA analysis. Transmission electron microscope (TEM) and energy dispersive X-ray spectroscopy (EDX) analysis were used to identify the microstructure and elements, respectively. The ion-exchange capacity of the prepared Tiron-grafted TiO_2 particles was measured by using a back-titration method. To do this, the powders were immersed in 1.0 M HCl solution for 24 h to convert all Na-form (-SO_3^--Na^+) to the H-form (-SO_3^--H^+). Thereafter, the resulting H-form powders were immersed again in 0.1 M NaOH solution for 24 h to completely replace the H^+ ions with the Na^+ ions, and the concentration of the remaining NaOH solution after removing the Tiron-grafted TiO_2 powders via a simple filtration was measured by a titration method using 0.1 M HCl solution and phenolphthalein as an indicator.

$$\mathrm{IEC[meq/g]} = \frac{0.1 \times (V_{NaOH} - V_{HCl})}{W} \quad (1)$$

where V_{NaOH} (mL) is the initial volume of 0.1 NaOH solution used to replace the H-form with the Na-form, V_{HCl} (mL) is the volume of 0.1 M HCl solution consumed for the titration, and W (g) is the weight of the dried Tiron-grafted TiO_2 sample. For the cation-exchange membrane, the ion-exchange capacity was evaluated by the same procedure.

3. Fabrication of Electrodes and Electrochemical Testing

Carbon electrodes of about 100 μm in thickness and 100 cm^2 (10 cm×10 cm) in area were fabricated on the graphite sheet via a doctor-blade method. Carbon paste was prepared by mixing AC powder (2.7 g) with Polyvinylidene fluoride (PVdF) (0.3 g) and N,N-Dimethylacetamide (DMAc) (7.0 g) using a planetary centrifugal mixer (Thinky mixer, ARE-310). Herein, the weight ratio of ACP : PVdF : DMAc was 27 : 3 : 70. The carbon paste was casted on the graphite sheet using a doctor blade, followed by a drying in a convection oven at 40 °C for 2 h. The Tiron-grafted TiO_2 layer on the prepared carbon electrode was formed by a screen printer (Automax, AMX-1240M) with a 200-mesh silk screen. The paste for the screen printing was prepared by mixing Tiron-grafted TiO_2 powder (3.0 g) with PVdF (1.3 g) and DMAc (12.9 g) in the weight ratio of powder : PVdF : DMAc=17.5 : 7.5 : 75. A schematic diagram for the fabrication of the Tiron-grafted TiO_2/carbon electrode is displayed in Fig. 1.

Cyclic voltammetry (CV) and electrical impedance spectroscopy (EIS) measurements were carried out in 0.5 M KCl solution using a three-electrode system to investigate the ionic-sorption capaci-

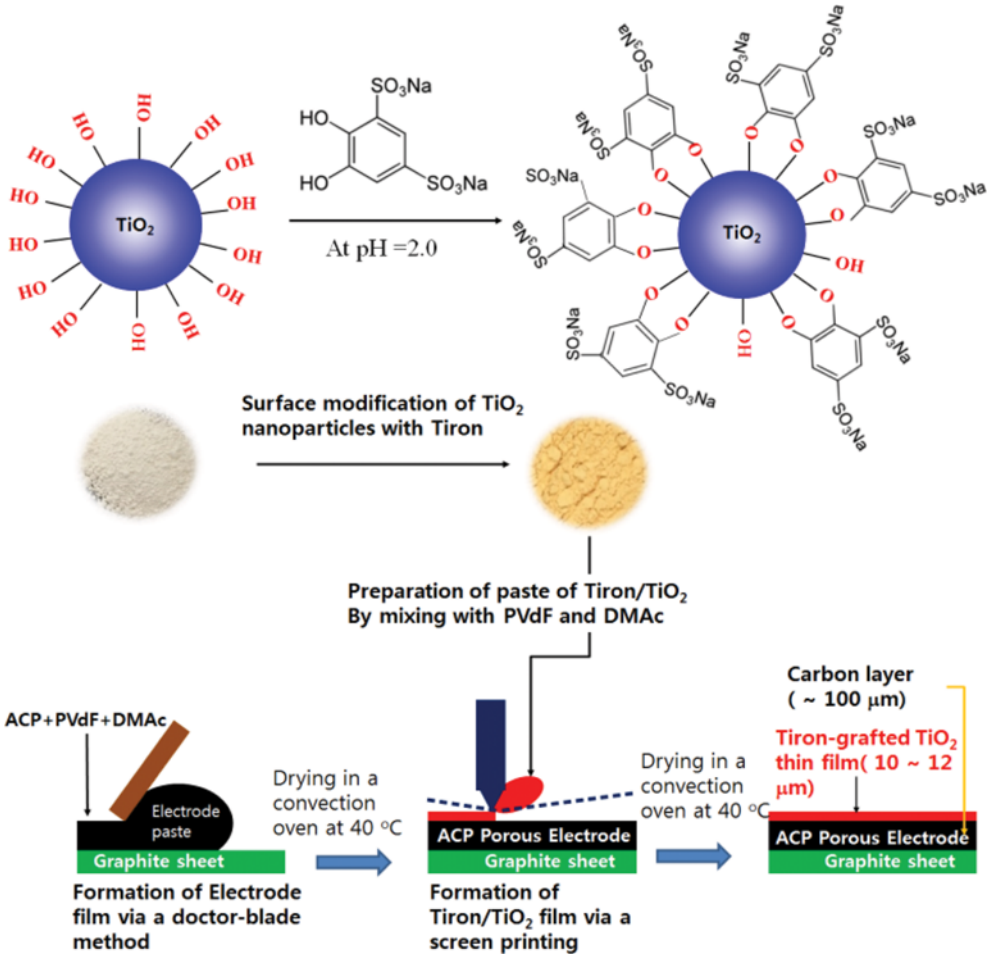

Fig. 1. Schematic diagram showing the preparation of Tiron-grafted TiO_2/carbon electrode.

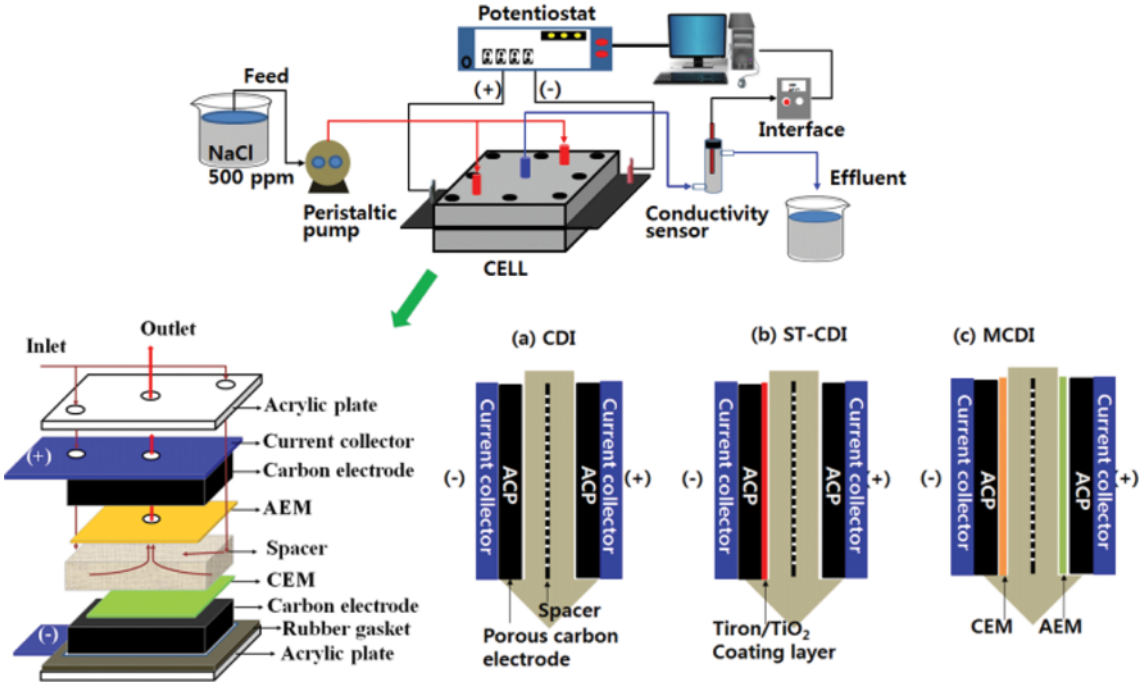

Fig. 2. Schematic diagram for the experimental setup to measure the deionization performance in CDI or MCDI unit cells.

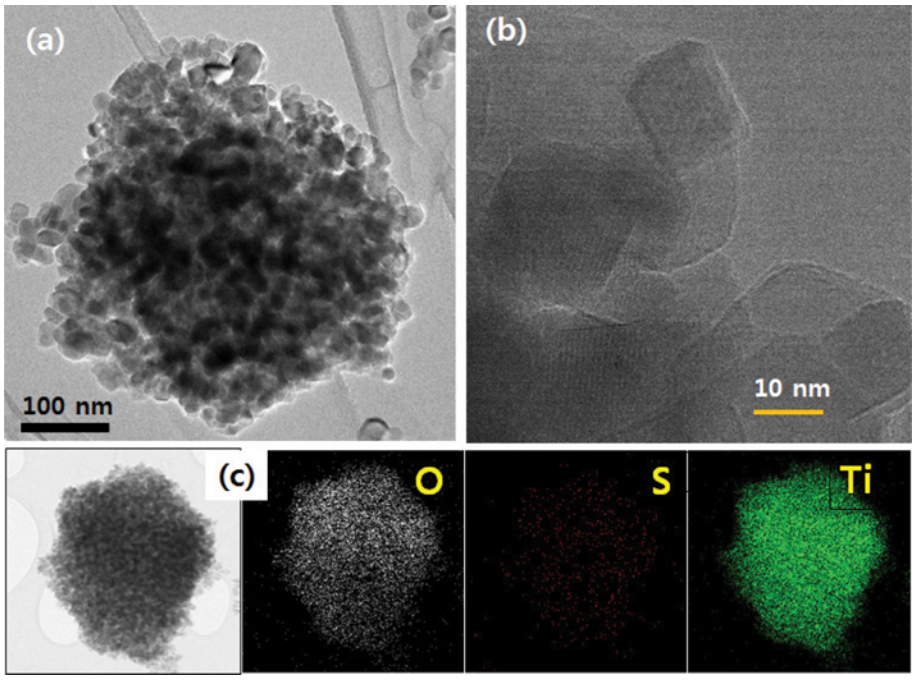

Fig. 3. TEM photos of Tiron-grafted TiO_2 nanoparticles (a) and (b), and element mapping results (c).

tance and electrochemical properties of the prepared electrodes. A carbon-coated platinum rode and an Ag/AgCl electrode were used as a counter and a reference electrode, respectively. Cyclic voltammetry was performed in the potential range from −0.5 V to 0.5 V (vs. Ag/AgCl) at the scan rate of 5-120 mV/s. The EIS measurement was conducted at the frequency range from 100 Hz to 10 mHz.

4. Deionization Evaluation

Fig. 2 shows the experimental setup used to evaluate the deionization performance of the electrodes prepared. The unit cell structures tested are included in Fig. 2. Three different unit cells were constructed called as CDI, ST-CDI and MCDI. A simple CDI unit cell consists of two carbon electrodes without the coating of Tiron-grafted TiO_2 or without the use of ion-exchange membranes. In the ST-CDI structure, the carbon film with the Tiron-grafted TiO_2 layer was used as the negative electrode and the positive electrode was prepared with the pure carbon. In the MCDI structure, ion-exchange membranes were inserted between two electrodes. That is, the cation-exchange membrane (CEM) was placed on the negative electrode and the anion-exchange membrane (AEM) was placed on the positive electrode. In all unit cells, a nylon-net spacer (100 μm) was inserted in the middle of both electrodes to from a flow path for the influent. The whole structure is shown in Fig. 2.

The influent was injected into the spacer through two holes placed at the edge of carbon electrode, and the desalinated water was ejected out through the hole in the center of the electrode. The influent (500 ppm NaCl aqueous solution) was supplied at a constant flow rate of 20 mL/min using a peristaltic pump. The conductivity of the effluent was monitored by a conductivity sensor (Model ET901, eDAQ) connected with a data logger (Model ED410, eDAQ). During the deionization experiments, the constant voltage (1.0 V) was applied to the CDI or MCDI cells using a potentiostat (ZIVA SP1).

RESULTS AND DISCUSSION

1. Tiron-grafted TiO_2 Nanoparticles

Fig. 3 shows TEM photos of TiO_2 nanoparticles obtained after the grafting of Tiron. The powder color changed from white (pure TiO_2) to dark yellow after the sulfonation, indicating the chemical adsorption of Tiron. TiO_2 powder used was aggregates of nano-sized primary particles of about 20-25 nm. The sulfonic groups in Tiron should remain on the surface titania nanoparticles without any chemical decomposition during the grafting process. To identify the sulfur element in sulfonic groups grafted titania, the EDX mapping was performed, and the results shown in Fig. 3(c). Element S is uniformly distributed in nano-sized TiO_2 aggregates, indicating that Tiron molecules are well grafted on the surface of titania nanoparticles.

The FT-IR measurement was conducted to confirm the presence of sulfonic groups, and the results are shown in Fig. 4(a). In both pure TiO_2 and Tiron-grafted TiO_2 samples, a narrow band at 1,620 cm^{-1} and a broad band around 3,400 cm^{-1} are observed, which are corresponding to the scissoring vibration of the stretching vibration of OH groups. For the Tiron-grafted TiO_2 sample, several new peaks appear. The C=C vibration peak is observed at 1,460 cm^{-1}, indicating the existence of benzene ring of Tiron [48]. Three new peaks at 1,270 cm^{-1}, 1,190 cm^{-1} and 1,030 cm^{-1} are attributed to the symmetric stretching of S=O, S-O and SO^{3-}, respectively. From the FT-IR peaks, it is clear that Tiron molecules are well grafted on the TiO_2 surface. Fig. 4(b) shows the TGA curves. At 700 °C, the weight loss difference between pure TiO_2 and Tiron-grafted TiO_2 is about 13.6 wt%. From the TGA result, the calculated loading of

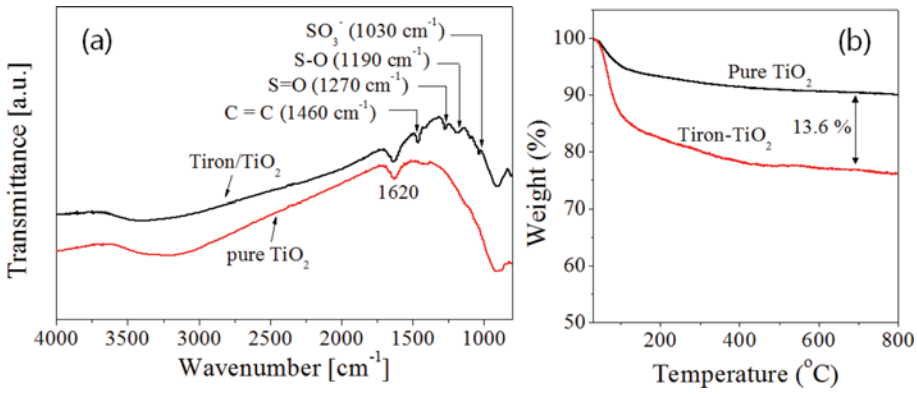

Fig. 4. (a) FT-IR spectra and TGA curves of pure TiO_2 and Tiron-grafted TiO_2 particles.

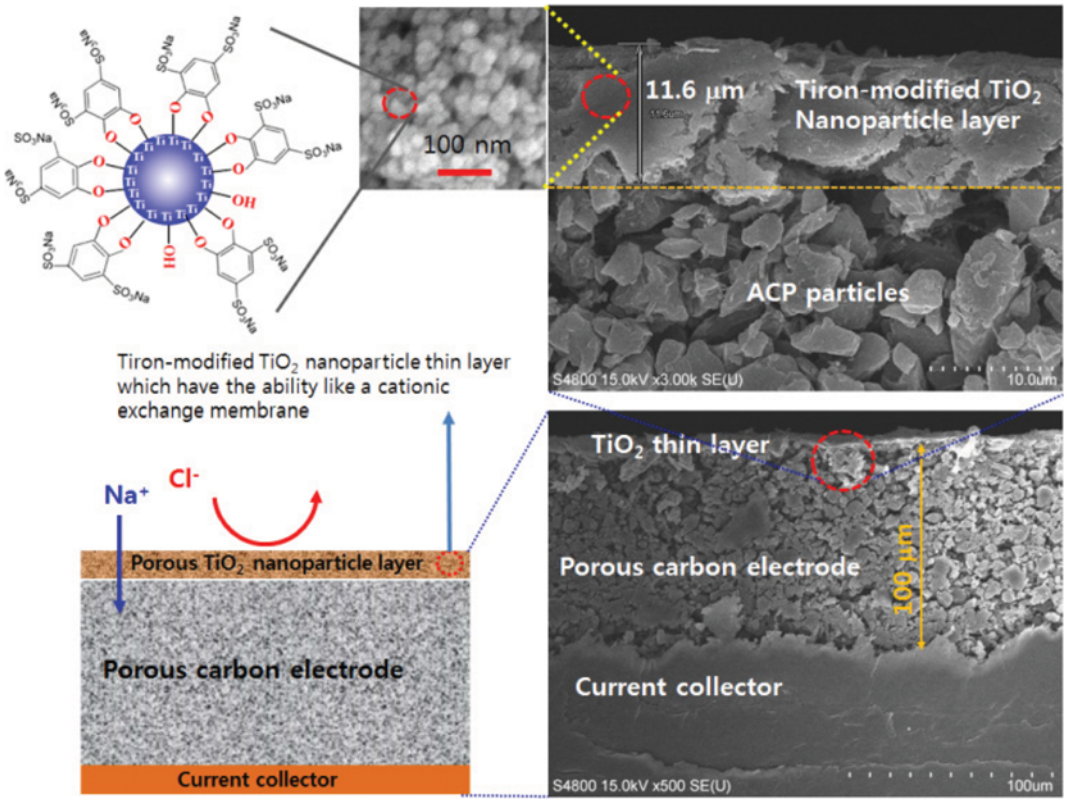

Fig. 5. Schematic diagram and SEM images for the cross section of the negative electrode of ST-CDI unit cell.

Tiron per 1 g TiO_2 is about 0.177 g Tiron/g-TiO_2. The grafting of Tiron was carried out in the HCl solution. Thus, the SO_3-Na groups in Tiron are transferred to the SO_3-H form. To completely transfer the SO_3-Na form to the SO_3-H form, the as-prepared Tiron-grafted TiO_2 powder was immersed in 1.0 M HCl solution for 24 h. Thereafter, the ion-exchange capacity evaluated by a titration method was about 1.51 meq/g. For the commercial cation-exchange membrane used in the MCDI cell, the ion-exchange capacity was measured by the same procedure and the resulting capacity was about 1.50 meq/g. From the results achieved so far, Tiron was successfully grafted on the nanosized TiO_2 surface, and the resulting particles were confirmed to have good ion-exchange capacity.

2. Deionization Characteristics

For three unit cells having different electrode structures as shown in Fig. 2, the deionization characteristics were evaluated in a continuous flow mode at 20 mL/min of 500 ppm NaCl solution. We compared the desalination performance of the ST-CDI structure with the conventional CDI or MCDI cells. Fig. 5 shows the schematic diagram and SEM images for the cross section of the negative electrode in the ST-CDI cell. The porous carbon layer has a thickness of about 100 μm. From the SEM results, the Tiron-grafted TiO_2 layer was confirmed to be well formed on the porous ACP layer with a thickness of 10-12 μm. This TiO_2 layer has also porous structure. Since the surface of TiO_2 nanoparticles were sul-

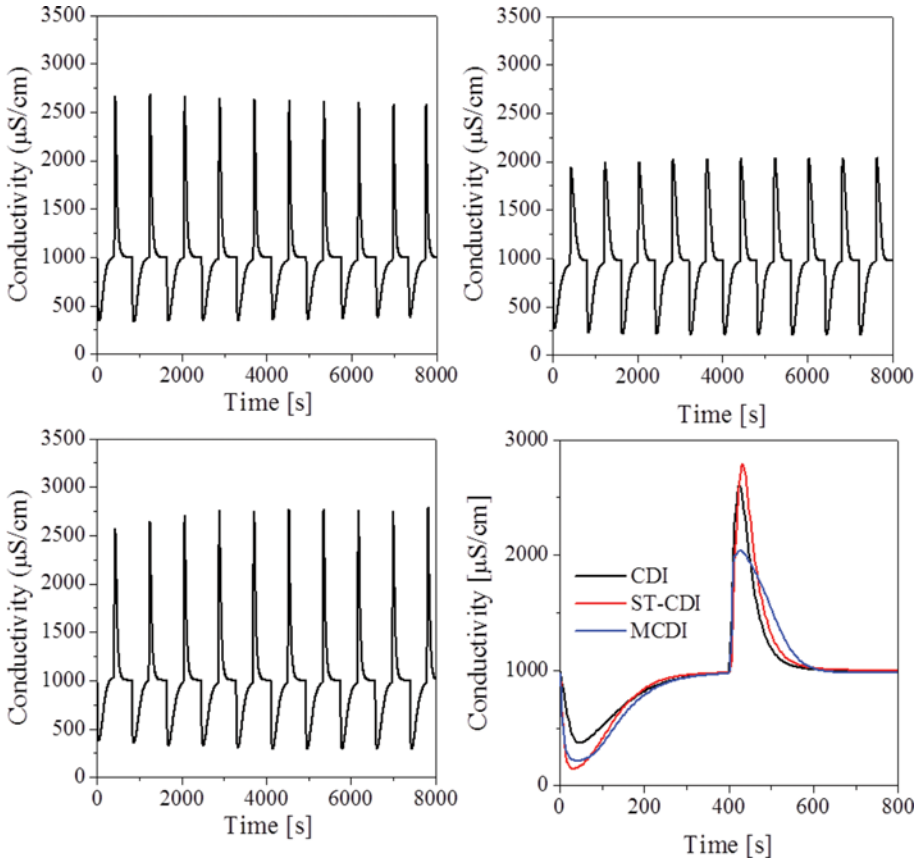

Fig. 6. Conductivity change of the effluent as a function of time, measured at the cell potential of 1.0 V. Repetitive adsorption-desorption cycles data for the cell of (a) CDI, (b) MCDI and (c) ST-CDI. (d) Comparison in the conductivity change at the 10th cycle.

fonated with Tiron, the pore channels within the TiO_2 top layer could penetrate cations, selectively.

For the prepared unit cells, ten cycles of adsorption-desorption experiments were carried out at 1.0 V flowing the NaCl solution (500 ppm) of 20 mL/min. The conductivity at the effluent was monitored as a function of time, and the resulting conductivity changes are shown in Fig. 6. When the cell potential was applied, the ion adsorption occurred quickly so that the conductivity at the effluent decreased steeply. After the conductivity reached a minimum value, it increased again up to the initial value. That is, the effluent concentration approached to the inlet concentration because of the limited adsorption capacity of the carbon electrode. Thereafter, the cell potential dropped to 0.0 V, immediately. As a result, the desorption occurred quickly, resulting in a sharp increment in the conductivity of the effluent. As the time increased in the desorption mode, the conductivity of the effluent also approached the initial value. These consecutive adsorption and desorption processes were repeated ten times. As shown in Fig. 6, the adsorption-desorption of NaCl occurred effectively in all the prepared unit cells and there was no significant difference in the cycle characteristics. From this cycle test, the coating of Tiron-grafted TiO_2 was identified to have no negative influence for the adsorption-desorption cycle property. To directly compare the desalination performance, the conductivity changes at the 10th cycle are shown in Fig. 6(d). In the adsorption period, the ST-CDI cell shows larger and sharper decrement in the conductivity than the pristine AC electrode (conventional CDI cell), which means that more ions are adsorbed and the adsorption becomes faster. Compared with the MCDI cell, the ST-CDI electrode has similar adsorption behavior. From this result, it is obviously confirmed that the Tiron-grafted TiO_2 layer is helpful for the substantial improvement in the desalination performance, and it successfully works like the cation-exchange membrane of MCDI. In the desorption step, the conductivity increase of the ST-CDI electrode is similar to the pristine AC electrode of CDI and sharper than the MCDI electrode. That is, the desorption of ions in the ST-CDI electrode takes place faster than in the MCDI electrode. This result is because the coated Tiron-grafted TiO_2 layer has a porous structure with the cation-exchange ability, whereas the ion-exchange membrane is relatively a dense film.

In the continuous cell operation, the salt quantity adsorbed on the electrode is a function of the operation time. That is, the NaCl quantity adsorbed on the carbon electrode varies with time. The adsorbed or desorbed NaCl quantity with time can be obtained by applying the unsteady-state material balance on NaCl in the CDI cell (accumulation=input−output).

$$\frac{dm}{dt} = V(C_0 - C) \tag{2}$$

where m is NaCl weight (mg), V (mL/min) is the volumetric flow

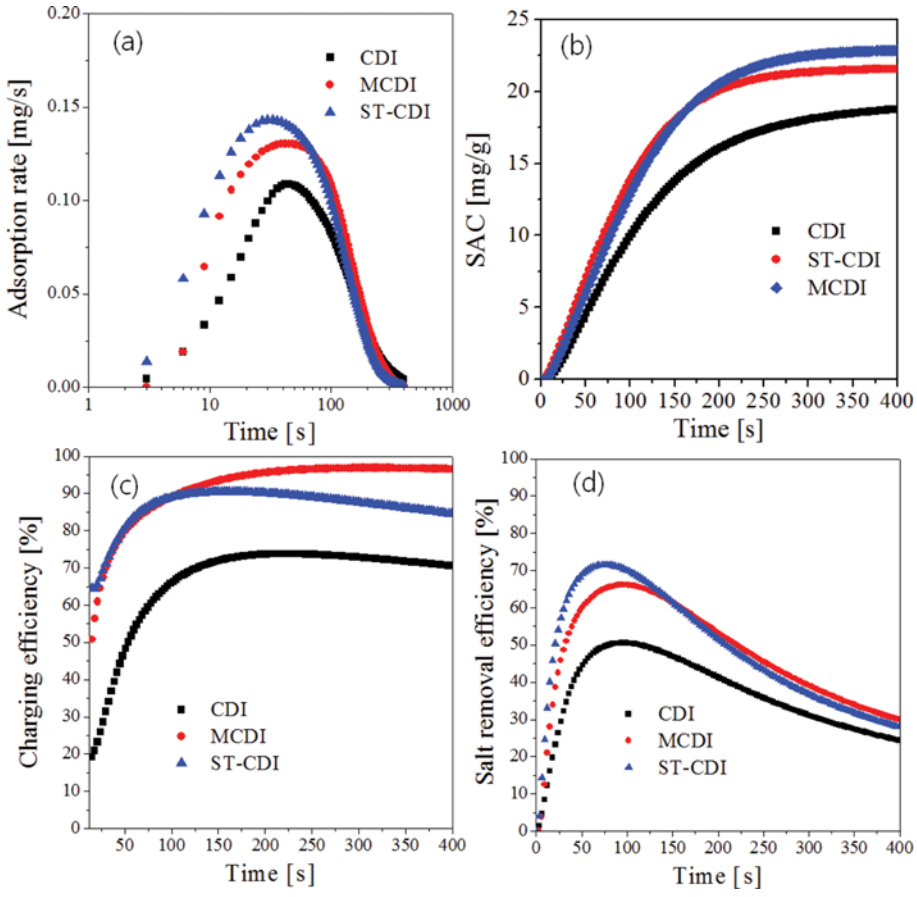

Fig. 7. (a) Adsorption rates calculated by the Eq. (2), (b) specific adsorption capacity, (c) current efficiency, and (d) salt removal efficiency as a function of time.

rate, which is constant at 20 mL/min in this work, C_0 (mg/L) is the influent concentration (500 mg/L) and *C* is the effluent concentration which changes with time. Then, the adsorption rate at an arbitrary time can be calculated by Eq. (2), and the results are shown in Fig. 7(a). The adsorption rate is much faster in the ST-CDI electrode or the MCDI electrode compared with the CDI electrode. The maximum adsorption rates of the CDI, MCDI and ST-CDI electrodes are 0.109 mg/s, 0.130 mg/s and 0.143 mg/s, respectively. That is, the maximal adsorption rate is enhanced about 1.3-times higher by introducing the Tiron-grafted TiO_2 layer on the porous ACP electrode. The desorption rate was also calculated, and the resulting values were 0.299 mg/s, 0.193 mg/s and 0.336 mg/s for the CDI, MCDI and ST-CDI electrodes, respectively. The desorption rate of the ST-CDI electrode is faster about 1.74 times than the MCDI electrode.

The specific adsorption capacity (SAC) is one of key factors in evaluating the performance of CDI electrodes. The cumulative adsorbed quantity can be obtained by integrating the instant adsorption rate with respect to the operation time. Then, the SAC can be calculated by the following equation:

$$SAC(mg/g) = \frac{V}{1000 W_C}\int_0^t (C_0 - C)dt \quad (3)$$

where W_C is the total mass of the carbon electrode. Fig. 7(b) shows the calculated SAC values with the operation time. The specific adsorption capacity was improved by coating the Tiron-grafted TiO_2 on the ACP layer. The equilibrium adsorption quantity of the ST-CDI electrode (21.5 mg/g-C) is 1.16-times higher than the CDI electrode (18.5 mg/g-C). The basic carbons of both the CDI electrode and the ST-CDI electrode are the same. Therefore, the improved SAC of the ST-CDI electrode reflects that the expulsion effect of co-ions is reduced by the Tiron-grafted TiO_2 layer having the cation-exchange ability.

Other key factors for evaluating the electrode performance are the specific adsorption rate (SAR) and the charging efficiency. The

Table 1. Summaries of the desalination performance and the electrochemical properties for the CDI, MCDI and ST-CDI electrodes

Cell types		CDI	MCDI	ST-CDI
Charging efficiency (η_C), %		73.8	95.6	90.6
Salt removal efficiency, %	Maximum	50.5	66.1	71.6
	Average	41.3	55.3	61.4
SAC, mg/g-C		18.5	22.7	21.5
SAR, mg/g-C/s		0.074	0.102	0.108
Specific capacitance, F/g		208	240	214
Charging resistance, mΩ		636	755	1344

SAR is easily obtained by dividing the SAC value with the operation time. As shown in Fig. 7(b), the SAC values increase with the operation time, and finally it becomes saturated. When the SAC value reaches 90% of the equilibrium, the SAR values obtained were summarized in Table 1. The average SAR values are 0.074, 0.102 and 0.108 mg/g/s for the CDI, MCDI and ST-CDI electrodes, respectively. Therefore, the SAR of the ST-CDI electrode is nearly the same as that of the MCDI electrode and about 1.5-times larger than the CDI electrode.

The ratio of total adsorbed ions to the total current passing through the cell during the operation time is defined as charging efficiency (η_C) [7]. Herein, the charging efficiency was calculated by the following equation:

$$\eta_C(\%) = \frac{\frac{V}{1000 M_{NaCl}} \cdot F \cdot \int_0^t (C_0 - C)dt}{\int_0^t I\, dt} \times 100 \quad (4)$$

where M_{NaCl} is the molecular weight of NaCl (58.44 g/mol), F is the Faraday constant (96485 C/mol), and I is the charging current at arbitrary times. The calculated charging efficiency is shown in Fig. 7(c). The charging efficiency increases sharply, reaches a maximum, and then decreases slightly with the adsorption time. Compared with the CDI and MCDI electrodes, the charging efficiency of the ST-CDI electrode reaches its maximum value in a short time and decreases relatively more. This is because the ion-adsorption saturation in the ST-CDI electrode occurs in a shorter time. Based on the time which the SAC value reaches 90% of the equilibrium, the efficiencies obtained are summarized in Table 1. The charging efficiency of the ST-CDI electrode is 90.6%, whereas the pristine AC electrode (CDI) is 73.8%. The enhanced charging efficiency of the ST-CDI electrode is attributed to the Tiron-grafted TiO_2 layer, which makes it possible for selective ion transport. The conventional MCDI cell has a charging efficiency of 95.6% due to the excellent selective transport of ions by the ion-exchange membranes. In terms of the charging efficiency, the ST-CDI electrode has about 95% performance compared with the conventional MCDI cell.

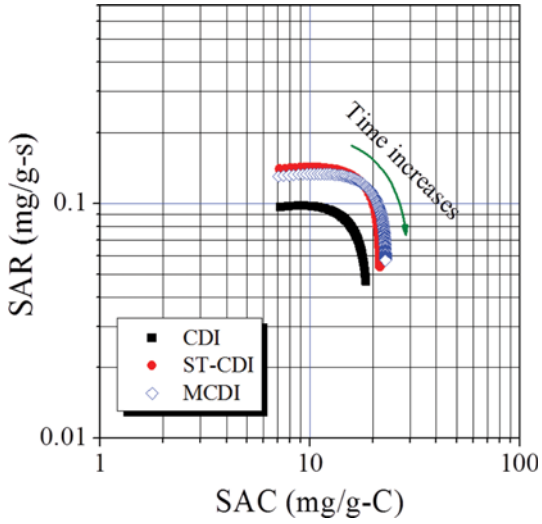

Fig. 8. Comparative Kim-Yoon plots for the CDI, ST-CDI and MCDI electrodes.

The salt removal efficiency (η_R) is a significant criterion for evaluating the capacitive deionization process, which is defined as the following equation [49,50]:

$$\eta_R(\%) = \left(1 - \frac{C_{eff}}{C_0}\right) \times 100 \quad (5)$$

where C_{eff} is the average concentration of NaCl in the effluent in the operation time. Then, the salt removal efficiency changes with the operation time as shown in Fig. 7(d). The efficiency increases sharply and reaches the maximum value within 100 s, and thereaf-

Table 2. Comparison of desalination performance of different electrodes: BM - batch mode, ACDI-asymmetric CDI and SP-single path mode

Electrode Materials	Functional group	Operation	C_0 [mg/L]	SAC [mg/g]	Potential [V]	η_C	Ref
Graphene//CFC[a]	SO_3^-	BM-MCDI	250	11	1.2	0.45	35
Graphene	NH_2/SO_3^-	BM-CDI	500	14	1.4	0.85	36
Graphene nanosheet	SO_3^-	BM-CDI	250	9	2		37
AAC[b]	ZnO	BM-CDI	1000	8	1.6	0.78	38
3DAPGr[c]		SP-CDI	300	14	1.4	0.82	39
3DAPGr	COO^{-2}/NR_4^+	SP-ACDI	300	23	1.4	0.85	39
AC	$C\text{-}N^+/C{=}O^-$	SP-CDI	500	21	1.2	0.68	40
AC		SP-CDI	500	19	1.0	0.79	40
		SP-MCDI	500	19	1.2	0.90	40
		SP-MCDI	500	15	1.0	0.85	40
AC		SP-CDI	500	19	1.0	0.74	This work
AC		SP-MCDI	500	23	1.0	0.96	This work
AC	TiO_2/SO_3^-	SP-CDI	500	22	1.0	0.91	This work

[a]CFC: carbon fibre cloth
[b]AAC: activated carbon cloth
[c]3DAPGr-3D activated microporous graphene

ter it decreases slowly with the operation time. The maximum salt removal efficiencies are given in Table 1. The maximum salt removal efficiency of the ST-CDI electrode (71.6%) is larger than that of CDI (50.5%) and MCDI (66.1%). The average removal efficiency calculated until the time which the SAC value reaches 90% of the saturation is summarized in Table 1. Based on these average values, the ST-CDI electrode shows about 49% improved salt removal efficiency compared with the CDI electrode and about 10% larger than the MCDI. Recently, Kim and Yoon suggested a new plot so called "Kim-Yoon plot" as CDI Ragone plot, which is a functional tool to evaluate the desalination performance [51]. Fig. 8 is the Kim-Yoon plot of the tested three electrodes. Ideally, the plot is placed at the upper part in the diagonal direction when the capacitive deionization processes have excellent performance. Thus, the ST-CDI electrode has desalination performance better than the CDI electrode and comparable with the MCDI electrode. Table 2 summarizes the desalination performance (SAC and charging efficiency) for surface-modified carbon electrodes reported in the previous literature. The charged functional groups mainly increase the hydrophilicity and improve the wettability of the carbon. Also, according to most reports, charged functional groups play a role in reducing co-ion expulsion, such as ion-exchange membranes. As a result, CDI performance has been reported to be improved by modifying the carbon surface with charged functional groups. Most previous reports have focused on directly modifying the carbon surface with charged functional groups including amines, sulfones, carboxylates and carbonyls. On the other hand, the ST-CDI electrode has a Tiron-grafted TiO_2 layer on the carbon electrode. As shown in Table 2, the ST-CDI electrode exhibits similar or superior desalination performance in specific adsorption capacity (SAC) or charging efficiency (η_C) compared with the direct modification of the carbon surface. Therefore, the use of Tiron-grafted TiO_2 nanoparticles as a functional layer can be considered as a simple and effective way to improve the CDI performance when using commercially available activated carbon as an electrode material.

3. Electrochemical Characteristics

To investigate the electrochemical behavior, the CV and EIS analyses were carried out, and the results are shown in Fig. 9. The pristine carbon used in the conventional CDI electrode was denoted as ACP. The negative electrodes of ST-CDI and MCDI were denoted as STC (sulfonated titania-coated carbon) and CEM (cation exchange membrane). Since the carbons used in all electrodes are ACP, all changes in the CV and EIS analysis are attributed to the coated Tiron-grafted TiO_2 layer in the ST-CDI electrode or the cation exchange membrane in the MCDI electrode. As shown in the

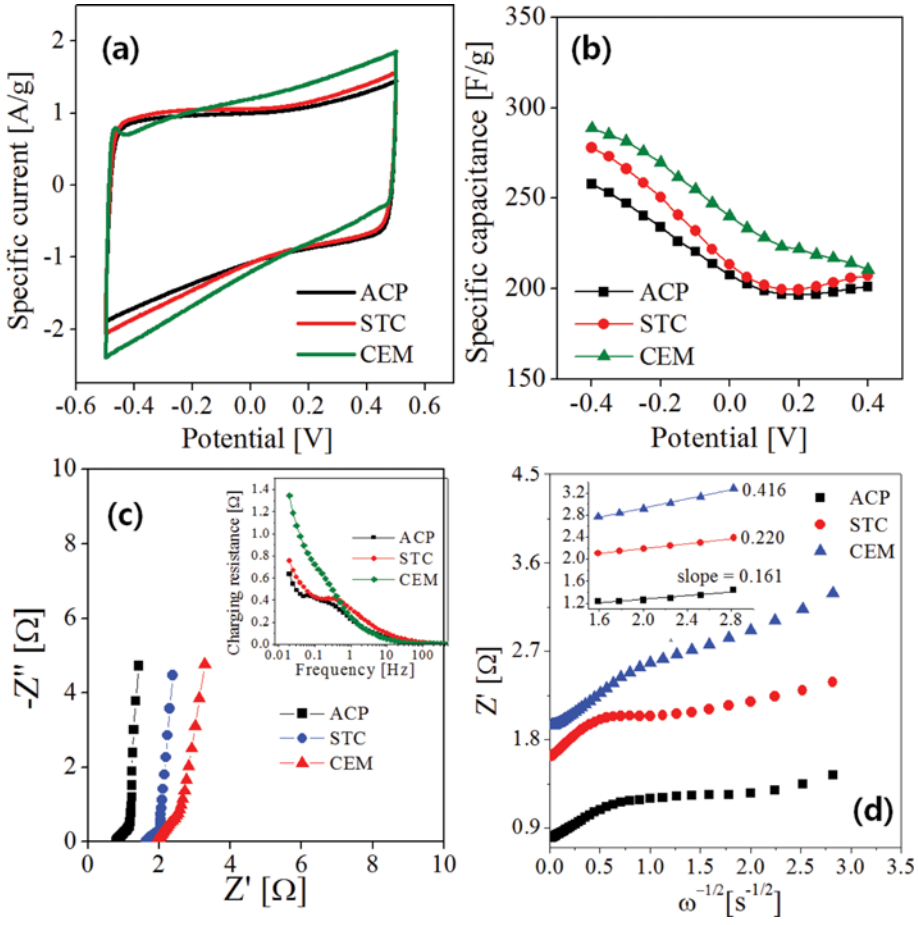

Fig. 9. (a) CV curves, (b) specific capacitances versus voltage, (c) Nyquist plots (inset - charging resistance), and (d) Randles plot (inset - linear fitting at low frequency).

CV data (Fig. 9(a)), all electrodes show a good CV curve observable in typical carbon-based electrical double-layer capacitors, and there is no Faradic reaction. The specific capacitance (C) was calculated from the CV data using the following equation [43].

$$C = \frac{I_a - I_c}{2vm} \quad (6)$$

where I_a and I_b are the anodic and cathodic current (A) at the voltage (v), respectively. m is the mass of carbon. The calculated specific capacitance values were displayed in Fig. 9(b) as a function of voltage. The coating of Tiron-grafted TiO_2 or the use of CEM improves the specific capacitance due to reduced co-ion repulsion, especially, in the negative voltage region. At +0.0 V, the specific capacitances are summarized in Table 1, which were 208, 240 and 214 F/g for ACP, CEM and STC, respectively. The improvement of specific capacitances of the STC or CEM electrode is in good agreement with the SAC values obtained in the full-cell experiments.

The electrochemical impedance spectroscopy (EIS) analysis was conducted to investigate the electrical behavior of electrode materials. Fig. 9(c) shows the Nyquist plots of the three electrodes. The straight spike of the Nyquist plots at the low frequency region is a typical curve observed in supercapacitors. The intercept of the real axis (Z′) corresponds to the equivalent series resistance including electrode, solution and contact resistance [52]. The intercept Z′ values are enlarged by the coating of Tiron-grafted TiO_2 or the use of CEM. Especially, the largest Z′ value of the CEM electrode is attributed to the free-standing ion-exchange membrane. The charging resistance can be calculated by the increase in the real part (Z′) of the impedance from the resistance at the highest frequency [53]. The calculated charging resistances are shown in the inset of Fig. 9(c), and the values at the frequency of 0.02 Hz are summarized in Table 1. Compared with the pristine ACP electrode (636 mΩ), both the STC (755 mΩ) and the CEM (1,344 mΩ) electrodes have higher charging resistance.

Warburg impedance (Z_W) is basically related to the diffusion of ions in porous carbon electrodes, which is expressed by the following equation [54]:

$$Z_W = \sigma \cdot \omega^{-1/2}(1-j) \quad (2)$$

where σ is the Warburg coefficient and w is the angular frequency ($2\pi f$). The Warburg coefficient has a relationship, $\sigma \propto D^{1/2}$, where D is ion diffusion coefficient in the porous electrode [55]. That is, the larger the Warburg coefficient, the slower the ion diffusion rate within the porous electrode. At high frequencies, the Warburg impedance is small or can be negligible because the ions do not have to move far. At low frequencies, however, the ions diffuse deeper into the pores, increasing the Warburg impedance. In a purely capacitive behavior, a completely vertical curve should be achieved in the Nyquist plot as the frequency decreases. As shown in Fig. 9(c), however, the real curve at low frequencies (1-0.01 Hz) deviates from the vertical line, indicating that there exists a diffusion limitation of ions into the inner pores. The ion diffusion property in the porous electrode can be identified from a Randles plot (Fig. 9(d)). The Warburg coefficient (σ) is equal to the slope of the Randles plot in the low frequency region, and the resulting values are 0.161, 0.220 and 0.416 $\Omega/s^{1/2}$ for the pure ACP, the STC and the CEM electrodes, respectively. That is, the introduction of a Tiron-grafted TiO_2 layer or the use of ion-exchange membrane increases the resistance of ion diffusion. In terms of the ion diffusion through the ion-exchangeable layer, clearly the Tiron-grafted TiO_2 layer (STC) is better than the cation exchange membrane (CEM). This result is in good agreement with the adsorption rate as shown in Fig. 7(a).

CONCLUSIONS

Tiron was grafted onto TiO_2 nanoparticles, and the resulting nanoparticles were used to form an ion-selective layer on the activated carbon layer. According to FT-IR and TEM/EDX analysis, Tiron grafting on TiO_2 surface was successfully accomplished. The Tiron-grafted TiO_2 was found to have good ion-exchange capacity comparable to commercial cation-exchange membranes. As a result, in the deionization experiment, the introduction of Tiron-grafted TiO_2 layer significantly made it possible to increase the ion adsorption capacity, charging efficiency, and salt removal efficiency without the use of the ion-exchange membrane. This enhancement in deionization performance reflects that the Tiron-grafted TiO_2 layer can work successfully as a cation-selective membrane and help reduce the co-ion repulsion effect. According to CV measurement, the specific capacitance of electrodes was improved by using the ion-selective layer such as the Tiron-grafted TiO_2 layer or the commercial ion-exchange membrane as the consequence of reducing the co-ion repulsion by the ion-selective layer. According to EIS analysis, the introduction of the Tiron-grafted TiO_2 layer resulted in the increase of the charging resistance or the ion diffusion resistance due to the interfacial resistance between the carbon layer and the TiO_2 layer. Clearly, the use of the Tiron-grafted TiO_2 layer as an ion-selective layer is better than the commercially available ion-exchange membrane in terms of lowering the ion diffusion resistance. Based on the results so far, it has been experimentally proved that the introduction of the Tiron-grafted TiO_2 layer as an ion-selective membrane is a simple and effective way to substantially increase the desalination performance.

ACKNOWLEDGEMENTS

This research was supported by Basic Science Research Program through the National Research Foundation of Korea (NRF) funded by the Ministry of Science, ICT & Future Planning (Grant No. 2015R1A2A2A03006558).

REFERENCES

1. T. J. Welgemoed and C. F. Schutte, *Desalination*, **183**, 327 (2005).
2. Y. Oren, *Desalination*, **228**, 10 (2008).
3. M. A. Anderson, A. L. Cudero and J. Palma, *Electrochim. Acta*, **55**, 3845 (2010).
4. S. Porada, R. Zhao, A. van der Wal, V. Presser and P. M. Biesheuvel, *Prog. Mater. Sci.*, **58**, 1388 (2013).
5. I. J. Esfanhani, J. Rashidi, P. Ifaei and C. Yoo, *Korean J. Chem. Eng.*,

33, 351 (2016).
6. R. Zhao, S. Porada, P. M. Biesheuvel and A. van der Wal, *Desalination*, **330**, 35 (2013).
7. M. E. Suss, S. Porada, X. Sun, P. M. Bieheuvel, J. Yoon and V. Presser, *Energy Environ. Sci.*, **8**, 2296 (2015).
8. C. Lian, K. Liu, K. L. Van Aken, Y. Gogotsi, D. J. Wesolowski, H. L. Liu, D. E. Jiang and J. Z. Wu, *ACS Energy Lett.*, **1**, 21 (2016).
9. Z.-H. Huang, Z. Yang, F. Kang and M. Inagaki, *J. Mater. Chem. A*, **5**, 470 (2017).
10. M. Wang, X. Xu, Y. Liu, Y. Li, T. Lu and L. Pan, *Carbon*, **108**, 433 (2016).
11. Y.-C. Tsai and R.-A. Doong, *Desalination*, **398**, 171 (2016).
12. R. Moradi, J. Karimi-Sabet, M. Shariaty-niassar and Y. Amini, *Korean J. Chem. Eng.*, **33**, 2953 (2016).
13. P. H. Kim and K. Y. Jung, *RSC Adv.*, **6**, 1686 (2016).
14. N. Jo, J.-H. Choi and K. Y. Jung, *J. Electrochem. Soc.*, **160**, E84 (2013).
15. L. Zou, G. Morris and D. Qi, *Desalination*, **225**, 329 (2008).
16. G. Wang, B. Qian, Q. Dong, J. Yang, Z. Zhao and J. Qiu, *Sep. Purif. Technol.*, **103**, 216 (2013).
17. Y. Bian, X. Yang, P. Liang, Y. Jiang, C. Zhang and X. Huang, *Water Res.*, **85**, 371 (2015).
18. J. Kim, D.-H. Peck, B. Lee, S.-H. Yoon and D.-H. Jung, *New Carbon Mater.*, **31**, 378 (2016).
19. P. Xu, J. E. Drewes, D. Heil and G. Wang, *Water Res.*, **42**, 2605 (2008).
20. R. Kumar, S. S. Gupta, S. Katiyar, V. K. Raman, S. K. Varigala, T. Pradeep and A. Sharma, *Carbon*, **99**, 375 (2016).
21. Y. Liu, G. Nie, L. Pan, X. Xu, Z. Sun and D. H. C. Chua, *Inorg. Chem. Front.*, **1**, 249 (2014).
22. H. Li, S. Liang, J. Li and L. He, *J. Mater. Chem. A*, **1**, 6335 (2013).
23. H. Li, Y. Ma and R. Niu, *Sep. Purif. Technol.*, **171**, 93 (2016).
24. H. Zhang, P. Liang, Y. Bian, Y. Jiang, X. Sun, C. Zhang, X. Huang and F. Wei, *RSC Adv.*, **6**, 58907 (2016).
25. X. Wen, D. Zhang, T. Yan, J. Zhang and L. Shi, *J. Mater. Chem. A*, **1**, 12334 (2013).
26. Z.-Y. Yang, L.-J. Jin, G.-Q. Lu, Q.-Q. Xiao, Y.-X. Zhang, L. Jing, X.-X. Zhang, Y.-M. Yan and K.-N. Sun, *Adv. Funct. Mater.*, **24**, 3917 (2014).
27. H. Yin, S. Zhao, J. Wan, H. Tang, L. Chang, L. He, H. Zhao, Y. Gao and Z. Tang, *Adv. Mater.*, **25**, 6270 (2013).
28. X. Xu, L. Pan, Y. Liu, T. Lu, Z. Sun and D. H. C. Chua, *Sci. Rep.*, **5**, 8458 (2015).
29. P. M. Biesheuvel, S. Porada, M. Levi and M. Z. Bazant, *J. Solid State Electrochem.*, **18**, 1365 (2014).
30. X. Gao, J. Landon, J. K. Neathery and K. Liu, *J. Electrochem. Soc.*, **160**, E106 (2013).
31. A. Omosebi, X. Gao, J. Landon and K. Liu, *ACS Appl. Mater. Interfaces*, **6**, 12640 (2014).
32. P. M. Biesheuvel and A. van der Wal, *J. Membr. Sci.*, **346**, 256 (2010).
33. R. Zhao, P. M. Biesheuvel and A. van der Wal, *Energy Environ. Sci.*, **5**, 9520 (2012).
34. J.-H. Lee and J.-H. Choi, *J. Membr. Sci.*, **409-410**, 251 (2012).
35. H. Li, F. Zaviska, S. Liang, J. Li, L. He and H. Y. Yang, *J. Mater. Chem. A*, **2**, 3484 (2014).
36. P. Liu, H. Wang, T. Yan, J. Zhang, L. Shi and D. Zhang, *J. Mater. Chem. A*, **4**, 5303 (2016).
37. B. Jia and L. Zou, *Chem. Phys. Lett.*, **548**, 23 (2012).
38. K. Laxman, M. T. Z. Myint, R. Khan, T. Pervez and J. Dutta, *Water Desalination*, **359**, 64 (2015).
39. A. G. El-Deen, R. M. Boom, H. Y. Kim, H. Duan, M. B. Chan-Park and J.-H. Choi, *ACS Appl. Mater. Interfaces*, **8**, 25313 (2016).
40. T. Wu, G. Wang, F. Zhang, Q. Dong, Q. Ren, J. Wang and J. Qiu, *Water Res.*, **39**, 30 (2016).
41. B. Qian, G. Wang, Z. Ling, Q. Dong, T. Wu, X. Zhang and J. Qiu, *Adv. Mater. Interfaces*, **2**, 1500372 (2015).
42. Y.-J. Kim and J.-H. Choi, *Water Res.*, **44**, 990 (2010).
43. J.-S. Kim and J.-H. Choi, *J. Membr. Sci.*, **355**, 85 (2010).
44. Y.-J. Kim and J.-H. Choi, *Water Res.*, **46**, 6033 (2012).
45. M. Moochani, A. Moghadassi, S. M. Hosseini, E. Bagheripour and F. Parvizian, *Korean J. Chem. Eng.*, **33**, 2674 (2016).
46. J. S. Kim, Y. S. Jeon and J. W. Rhim, *Sep. Purif. Technol.*, **157**, 45 (2016).
47. X. Gao, A. Omosebi, N. Holubowitch, A. Liu, K. Ruh, J. Landon and K. Liu, *Desalination*, **399**, 16 (2016).
48. T. Xu, W. Hou, X. Shen, H. Wu, X. Li, J. Wang and Z. Jiang, *J. Power Sources*, **196**, 4934 (2011).
49. H. Li, Y. Gao, L. Pan, Y. Zhang, Y. Chen and Z. Sun, *Water Res.*, **42**, 4923 (2008).
50. Y.-J. Kim and J.-H. Choi, *Sep. Purif. Technol.*, **71**, 70 (2010).
51. T. Kim and J. Yoon, *RSC Adv.*, **5**, 1456 (2015).
52. D. Zhang, T. Yan, L. Shi, Z. Peng, X. Wen and J. Zhang, *J. Mater. Chem.*, **22**, 14696 (2012).
53. B.-H. Park and J.-H. Choi, *Electrochim. Acta*, **55**, 2888 (2010).
54. A. Singh and A. Chandra, *Sci. Rep.*, **6**, 25793 (2016).
55. S.-K. Kim and H. S. Park, *RSC Adv.*, **4**, 47827 (2014).